FISEVIER

Contents lists available at ScienceDirect

Palaeogeography, Palaeoclimatology, Palaeoecology

journal homepage: www.elsevier.com/locate/palaeo





Yilong lake level record documents coherent regional-scale changes in Holocene water balance in Yunnan, southwestern China

Aubrey L. Hillman ^{a,*}, Angelena N. Campisi ^a, Mark B. Abbott ^b, Daniel J. Bain ^b, Melissa P. Griffore ^b, Rebecca A. Tisherman ^b, Zijie Yuan ^c, Duo Wu ^c

- a Department of Atmospheric and Environmental Science, University at Albany, State University of New York, 1400 Washington Ave, Albany, NY 12222, USA
- ^b Department of Geology and Environmental Science, University of Pittsburgh, 4107 O'Hara St, Pittsburgh, PA 15260, USA
- ^c College of Earth and Environmental Sciences; MOE Key Laboratory of Western China's Environmental Systems, Lanzhou University, Lanzhou 730000, China

ARTICLE INFO

Editor: Paul Hesse

Keywords:
Holocene
Paleoclimatology
Carbonate stable isotopes
Indian Summer Monsoon
Elemental ratios
Human-environmental interactions

ABSTRACT

Although Holocene-scale trends in Indian Summer Monsoon (ISM) variability have been well-established, manifestations and drivers of centennial- and multi-decadal-scale variability are still debated. Additionally, the extent to which proxies reflect abrupt climatic changes rather than proxy-specific thresholds is unclear. To address these questions, we summarize a 9200-year record from Yilong Lake in Yunnan China using multiple proxies including oxygen and carbon isotopes of authigenic calcite as well as Ti/Al ratio to characterize lake hydrologic balance and catchment erosion, respectively. We compare these results to two other well-studied nearby lakes on the Yunnan Plateau. At all three lakes, the Holocene-scale waning of the ISM is evident, but punctuated by abrupt shifts indicative of lower precipitation and/or greater evaporation at 7900, 5500, and 4500 cal yr B.P. We suggest that a shift to a positive mean-state of the Indian Ocean Dipole lasting multiple centuries can account for these events, with possible moderating influence from El Niño Southern Oscillation. After 1500 cal yr B.P., Yilong oxygen isotopes shift to less negative values as a result of human manipulation of hydrologic balance, coincident with the deposition of a red clay layer from catchment erosion. These results are similar to other Yunnan lakes although the intensity of anthropogenic management of Yilong's hydrologic balance is substantially smaller than at the other regional lakes. These results underscore the diversity of anthropogenic impacts to lakes, even ones that are only a few kilometers apart, and demonstrate spatiotemporal differences in freshwater resource use.

1. Introduction

The Indian Summer Monsoon (ISM) provides vital freshwater to India, China, and other parts of heavily populated Southeast Asia. Ongoing climate change will result in increased interannual extremes (Sharmila et al., 2015), therefore understanding how the ISM interacts with internal climate modes is vital for predicting the range of potential extremes. It is well-established that as summer insolation declined through the Holocene, so too did the strength of the ISM (e.g., Bird et al., 2014; Cheng et al., 2012; Contreras-Rosales et al., 2014; Fleitmann et al., 2007; Kudrass et al., 2001) in accordance with Kutzbach's hypothesis (Kutzbach, 1981); however, shorter-term centennial and decadal-scale variability during this period became more spatially variable. Some records find evidence for periods of aridity associated with North Atlantic events (Cai et al., 2012; Fleitmann et al., 2003; Gupta et al.,

2002), while others identify evidence for abrupt shifts in aridity that can be mechanistically linked to Pacific or Indian Ocean sea surface temperatures (Berkelhammer et al., 2012; Griffiths et al., 2020; Prasad et al., 2014). Further investigation of the spatial and temporal coherence of pluvial/arid periods on centennial and decadal timescales are the most informative for assessing changes in hydrologic balance over the course of human lifetimes. Similarly, it is crucial that we document the timing and magnitude of pre-industrial human exploitation of water resources in order to understand the context of more recent environmental challenges.

In the Yunnan Province of Southwestern China, there are numerous lakes (Dian, Xingyun, Qilu, Yilong, Fuxian; Fig. 1B) that can be used to reconstruct hydroclimate. Previous research in Yunnan has focused on palynology (Chen et al., 2014; Xiao et al., 2017; Xiao et al., 2014; Xiao et al., 2020; Xu et al., 2017) and oxygen isotopes (Hillman et al., 2017;

E-mail address: ahillman@albany.edu (A.L. Hillman).

^{*} Corresponding author.

Hillman et al., 2020; Hodell et al., 1999; Wu et al., 2018). While both proxies document the Holocene ISM decline, the timing and magnitude of centennial- and multi-centennial-scale abrupt shifts is at times coherent amongst lakes and at other times disparate. This suggests that either lakes and their catchments have differing sensitivities or there are proxy-specific thresholds that are crossed in response to gradual climate forcing. Additional records from catchments with a range of hydrologic sensitivities can therefore serve to distinguish between these two options. It is also clear from previous work that anthropogenic disturbances vary in the timing of onset as well as magnitude. Generally speaking, sediment core studies detect impacts to catchment vegetation earlier than either agriculture and consequent soil erosion or intensive manipulation of lake hydrology such as trenching and damming. However, each watershed has unique characteristics making the registry of these events in the sediment record somewhat site-specific. Understanding the specificity of these impacts is important to generating predictive tendencies at other locations where dense sampling cannot be performed.

Here we focus on Yilong Lake in southern Yunnan Province, approximately 150 km from Kunming, the provincial capital (Fig. 1B). Yilong is in close proximity to lakes Xingyun (Chen et al., 2014; Hillman et al., 2017; Hodell et al., 1999) and Oilu (Hillman et al., 2020; Hodell et al., 1999) both of which have published oxygen isotope records and lend themselves to comparison, but differing morphometric characteristics, residence times, and evaporative enrichment of oxygen isotopes (Table 1). A previous publication on Yilong (Yuan et al., 2021) used a multi-proxy approach and focused on characterizing a period of low lake levels centered on 9300 cal yr B.P. and contrasting the ecological response of this event with human activities after 1500 cal yr B.P. We present here a follow-up study of Yilong with added radiocarbon dates, a new age-model, and high-resolution $\delta^{18}O$ sampling with the intent of explicitly reconstructing water balance. Our objective here is to produce a multi-proxy estimate of lake levels through the Holocene to examine abrupt shifts in hydroclimate in Yunnan. We also aim to characterize the timing, magnitude, and scope of human impacts to lake hydrologic balance in the region.

2. Background

2.1. Regional climate and precipitation isotopes

Yunnan climate is humid sub-tropical (Kottek et al., 2006) with warm temperatures year-round and a precipitation regime dominated by the ISM with 70% of the mean annual total accumulating during the months June–September (IAEA/WMO, 2018) (Fig. 2A). Although most precipitation arriving in Yunnan is delivered by the ISM, undoubtedly some portion of moisture is associated with the East Asian Summer Monsoon (EASM), particularly during the decay of the monsoon season (Hillman et al., 2017). On orbital timescales, the ISM responds to Northern Hemisphere summer insolation with a particular dominance in the precessional band (Liu et al., 2006). It is therefore well-established that the early Holocene was a time of enhanced monsoon precipitation while the late Holocene was characterized by diminished monsoon precipitation (Wang et al., 2017; Wu et al., 2018).

The isotopic composition of precipitation in Kunming tends to have more negative oxygen and hydrogen values in the summer (IAEA/WMO, 2018) (Fig. 2A) due to upstream air mass processes such as rain-out and convection that occur along the air mass travel path (Vuille et al., 2005). Temperature is generally considered to have a negligible effect on precipitation isotopic composition in Kunming (Araguas-Araguas et al., 1998). Due to the summer dominance of precipitation that has a more negative isotopic composition than the winter, the average weighted value of oxygen isotopic composition in precipitation is -9.9% VSMOW (Fig. 2B). While our study site of Yilong is 150 km south of Kunming, we assume that these general trends and values of precipitation isotopes are the same between the two locations.

2.2. Lake background

Yilong Lake is part of a sag pond along the Jianshui fault (Wang et al., 1998) and has a surface area of approximately $31~\mathrm{km}^2$ with a watershed area of $360~\mathrm{km}^2$ (Bai et al., 2011) (Fig. 1C). The average depth of the lake is 2.8 m and the maximum depth is 6.2 m (Whitmore et al., 1997). However, LANDSAT images show that from 2013 to 2016 the lake level

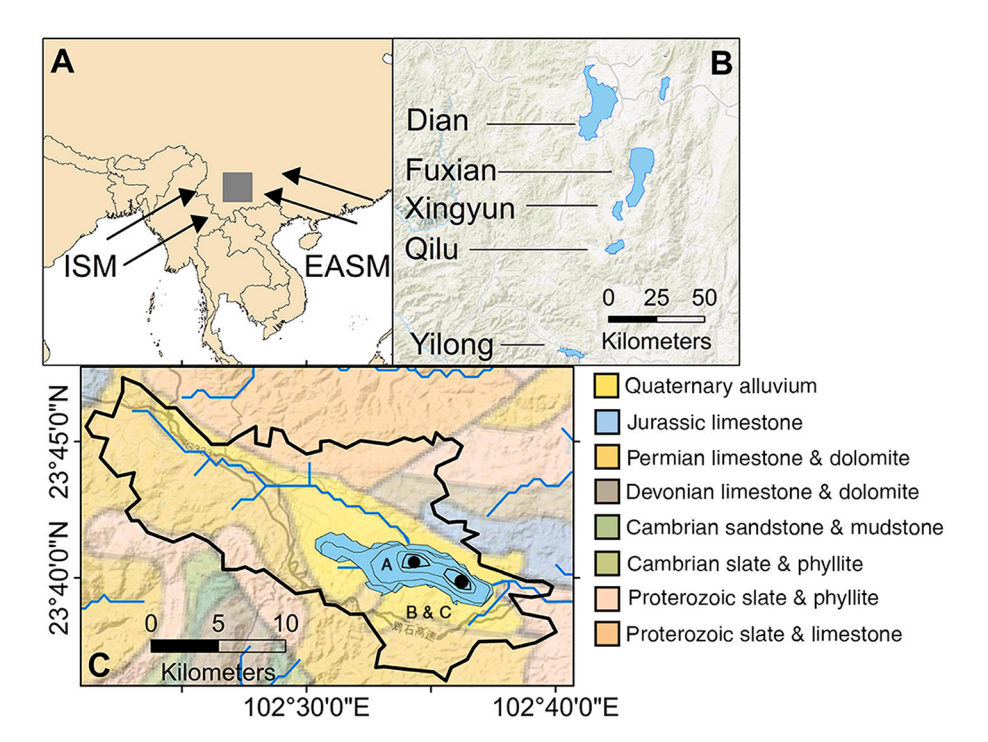


Fig. 1. A- Yilong Lake (gray square) with generalized direction of ISM and EASM winds; B) central Yunnan lakes; C) Yilong catchment (black border) and geology (Province Bureau of Geology and Mineral Resources of Yunnan). Coring locations are marked by black circles. Lake bathymetry is a 1 m contour interval.

Table 1-Characteristics of Yunnan lakes discussed in this study.

Lake	Max depth (m) ^a	Mean depth (m) ^a	Surface area (km²) ^b	Catchment area (km²) ^b	Volume (x 10 ⁶ m ³) ^b	Catchment: surface area ratio	δ^{18} O value in 1997 (‰ VSMOW) ^a	δ^{18} O value in 2019 (‰ VSMOW)
Xingyun	9.8	2.9	34	383	201	11.2	-5.7	-4.3
Qilu	6.8	4.0	36	200	200	5.5	-5.9	-4.3
Yilong	6.2	2.8	31	360	90	11.6	-4.3	-3.5

^a Whitmore et al., 1997.

^b Determined via ASTER global Digital Elevation Maps and lake bathymetry data.

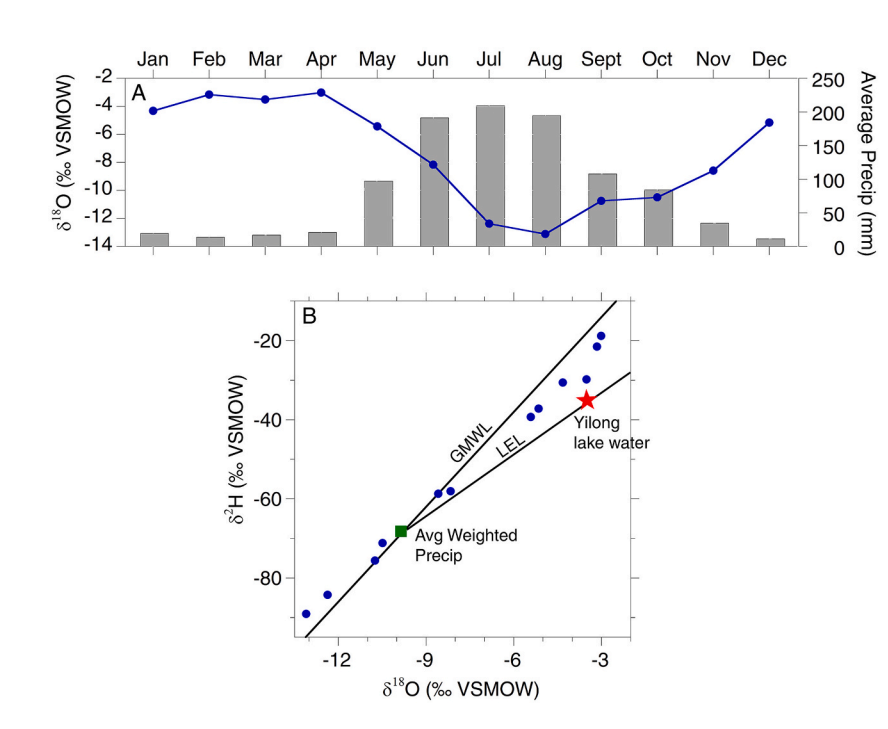


Fig. 2. A) Average monthly precipitation amount (gray bars) and isotopic composition of precipitation (blue circles) for Kunming from 1986 to 2003 CE. B) Average monthly $\delta^{18}\text{O}$ versus δD isotopic composition of precipitation (blue circles). The global meteoric water line (GMWL) and the local evaporation line (LEL) are shown. The green square is the average weighted composition of Kunming precipitation and the red star is Yilong lake water from 2019. (For interpretation of the references to colour in this figure legend, the reader is referred to the web version of this article.)

dropped by several meters and surface area was around 50% less as compared to prior and subsequent periods (Fig. S1). The lake has one inflowing river from the west and one outflowing river to the east (Fig. 1C). Although it is hydrologically open, the isotopic composition of lake water in summer 2019 was less negative (-3.5% VSMOW) when compared to the annual weighted mean of Kunming precipitation (-9.9% VSMOW), strongly suggesting that water loss via evaporation is substantial (Fig. 2), and that the lake functions as a closed basin. While our measurement of the isotopic composition of lake water was only one year, previous measurement in 1997 found a value of -4.3% VSMOW (Whitmore et al., 1997), consistent with substantial evaporation. Modification of the lake shoreline due to the agricultural practices, particularly rice, is apparent in the southwest (Fig. S1). The bedrock geology of the catchment is dominated by Permian limestone and dolomite with small portions of Jurassic limestone, Devonian limestone and dolomite, and Proterozoic slate, phyllite, and limestone (Bureau of Geology and Mineral Resources of Yunnan Province, 1990) (Fig. 1C).

We primarily compare Yilong to nearby lakes Xingyun and Qilu, both of which also function as closed basins. Adjacent closed basin lakes may experience similar hydrologic forcings but exhibit slightly different responses due to morphometry and water residence time (Steinman et al., 2010). Compared to Xingyun and Qilu, Yilong has a similar surface area as well as sensitivity to evaporative water loss (Table 1). However, the three lakes are expected to exhibit differing water residence times due to variations in depth and volume. Xingyun is the largest and deepest and accordingly is expected to have the longest water residence time. Yilong is the smallest and shallowest and likely has the shortest residence time. Catchment to surface area ratio will also influence the hydrologic

response time of each lake. Xingyun with the largest catchment to surface area likely has a dampened response while Qilu with the smallest catchment to surface area likely responds more rapidly.

3. Materials and methods

3.1. Core collection

Three sets of cores (A-19, B-19, and C-19) were collected in May 2019 using a steel barrel Livingston corer (Wright et al., 1984) from the two deepest parts of the lake (A-19: 23°40′41.8″N, 102°34′29.6″E, B-19 and C-19: 23°39′41.4″N, 102°36′12.6″E) (Fig. 1C). B-19 and C-19 are parallel cores from adjacent locations. Each set of cores consists of 1-m long drives that were collected in overlapping sections. The A-19 cores comprise a 228 cm long record, the B-19 cores a 332 cm record, and the C-19 cores a 338 cm record. Overlapping sections of 1-m long drives were correlated on the basis of field notes and sediment geochemistry (such as weight percent carbonate and $\delta^{18}O$ values). Additionally, surface cores that preserved the sediment-water interface were collected using a lightweight percussion coring system. These surface cores were extruded in the field at 0.5 cm intervals. The three sets of cores were correlated to each other on the basis of sedimentology, weight percent organic matter, and weight percent carbonate (Fig. S2 and 3). A-19 and C-19 cores were correlated to the B-19 core depths since B-19 has the high-resolution isotope data and the majority of our analysis and interpretation focuses on the B-19 cores.

3.2. Age control

Radiocarbon ages were measured on nine samples of charcoal, aquatic and terrestrial plant macrofossils, and wood from the B-19 cores and thirteen samples of charcoal and aquatic and terrestrial plant macrofossils from the C-19 cores (Table 2). Samples were pretreated using a standard acid, base, acid procedure (Olsson, 1986) and processed and analyzed at the W.M. Keck Carbon Cycle Accelerator Mass Spectrometry Laboratory at the University of California, Irvine (B-19) and Beta Analytic (C-19). The resulting ages were calibrated using CALIB 8.2 and the INTCAL20 calibration curve (Reimer et al., 2020). The upper 30 cm of the B-19 surface core sediments were lyophilized and analyzed for 210 Pb and 214 Pb activities by direct gamma (γ) counting in a broad energy germanium detector (Canberra BE-3825) at the University of Pittsburgh. Sediment ages for the surface were calculated using the Constant Rate of Supply (CRS) method, which accounts for variability in sediment flux, according to the methodology of (Binford, 1990) (Table S1). An age-depth model was developed using the ²¹⁰Pb ages and calibrated radiocarbon dates. The resulting calibrated dates were used in the BACON code which uses Markov chain Monte Carlo statistics to create age-depth models and uses posterior probabilities to determine radiocarbon outliers (Blaauw and Christen, 2011) in the statistical software package "R" (R Core Development Team, 2008).

3.3. Geochemistry

Density and loss-on-ignition (LOI) were measured at 2-cm intervals on the B-19 cores using 1 cm³ samples. Samples were dried at 60 °C for 48 h to remove water and weighed for dry bulk density. Weight percent organic matter content was determined by LOI at 550 °C and percent carbonate by LOI at 1000 °C (Dean, 1974). The B-19 core sequence was sampled at 0.5–2.0 cm intervals for $\delta^{18}\text{O}$ and $\delta^{13}\text{C}$ values. Approximately 10 samples from each drive were analyzed through overlapping sections to check for consistency. Samples were disaggregated with 7% H_2O_2 and sieved through a 63-µm screen to remove biological carbonates derived from shells. The resulting fine-grained carbonate sediment was oxidized with a dilute (~3%) bleach solution, rinsed three times with Milli-Q water, frozen, lyophilized, and homogenized using an agate mortar and pestle. Bulk carbonate samples were reacted in ~100% phosphoric acid under vacuum at 70 °C. Samples were measured using an automated carbonate preparation device (KIEL-III) coupled to a gas-

ratio mass spectrometer (Finnigan MAT 252) at the Environmental Isotope Laboratory, University of Arizona. Measurements were calibrated to the NBS-18 and NBS-19 calcite standards and values are reported in standard delta (δ) notation as the per mil (∞) deviation from Vienna Pee Dee Belemnite (VPDB). One sigma analytical uncertainties on the standards are within $\pm 0.10\%$ for δ^{18} O and \pm 0.08% for δ^{13} C.

Samples for powder X-ray diffraction (XRD) analysis were taken every 50 cm on the B-19 cores, lyophilized, and homogenized with an agate mortar and pestle. The samples were prepared as back-filled cavity mounts and analyzed using a Rigaku Smart Lab X-ray Diffractometer to identify the carbonate mineral phase (Cu anode, 40 kV, 45 mA, from 5 to 80° at 0.02 step width, $10^{\circ}/\text{min}$). Samples were also analyzed on a Hitachi S3000N Scanning Electron Microscope (SEM) to examine crystal structure and morphology.

Samples for weight percent nitrogen, weight percent organic carbon, and atomic carbon to nitrogen (C/N) ratio were taken at 1 or 2-cm intervals from the B-19 cores and acidified with 1 M HCl to remove carbonate material. Samples were then rinsed to neutral and analyzed at the University of Pittsburgh using an ECS 4010 (Elemental Combustion System 4010) interfaced to a Delta V mass spectrometer through the ConFlow IV system.

Drives 1 through 3 of the A-19 cores were analyzed via scanning X-ray fluorescence (XRF) at 1 mm resolution at the University of Minnesota Duluth, Large Lakes Observatory. XRF measurements do not continue to the uppermost sediments because the surface core was extruded into bags and therefore could not be scanned. Since changes in organic matter can influence XRF measurements, we normalize elements to Al, a standard method (Löwemark et al., 2011).

4. Results

4.1. Geochronology

The Bacon age model suggests that the 332 cm of B-19 core section spans 10,100 cal yr B.P. (Fig. 3). This may be an underestimation of the age of the base of the core since one radiocarbon date from 314.5 cm dates to \sim 12,500 cal yr B.P. Bacon likely underestimates the age because it incorporates information about sedimentation rates throughout the core and the basal date would imply a much slower sedimentation rates below 300 cm than the rest of the core. Slow sedimentation rates are plausible during dry conditions and reduced sediment influx or during

Table 2AMS radiocarbon dates from Yilong cores.

Core	ID#	Adjusted Core Depth (cm)	Material	¹⁴ C age (BP)	Error ±	Median Probability Calibrated Age (yr BP)	2σ Calibrated Age Range (yr BP)
C19	535,118	32.5	Aquatic plants	890	30	783	728 to 832
B19	224,791	36.5	Charcoal	510	20	529	511 to 545
B19	224,792	48.5	Wood, charcoal, seed husks	1440	20	1330	1300 to 1356
B19	224,605	51.0	Charcoal	1460	20	1345	2752 to 3300
C19	535,120	63.0	Charcoal	2610	30	2645	2719 to 2769
B19	224,793	69.5	Charcoal	2850	120	2993	1306 to 1375
C19	535,121	80	Terrestrial plants	2820	30	2921	2848 to 3004
B19	224,606	83.5	Charcoal	2710	20	2806	2761 to 2850
C19	535,123	97.4	Aquatic plants	3520	30	3782	3698 to 3879
C19	535,124	114.5	Aquatic plants	4250	30	4836	4813 to 4864
B19	224,607	118.0	Aquatic plants	4110	25	4626	4524 to 4812
C19	535,125	156.5	Aquatic plants	4820	30	5522	5477 to 5539
B19	224,608	181.0	Aquatic plants	4760	20	5526	5468 to 5582
C19	535,126	183.3	Aquatic plants	5000	30	5723	5650 to 5760
C19	535,127	203.5	Aquatic plants	5700	30	6478	6401 to 6562
C19	535,128	223.5	Aquatic plants	6240	30	7168	7186 to 7254
C19	535,130	253.5	Aquatic plants	6360	30	7284	7246 to 7331
B19	224,609	265.5	Wood	7310	30	8108	8030 to 8177
C19	535,131	268.5	Aquatic plants	6990	30	7824	7728 to 7874
C19	535,132	287.35	Terrestrial plants	7860	30	8634	8585 to 8771
B19	224,610	295.5	Charcoal	8930	90	10,025	9722 to 10,238
C19	535,133	314.5	Terrestrial plants	10,470	40	12,493	12,431 to 12,620

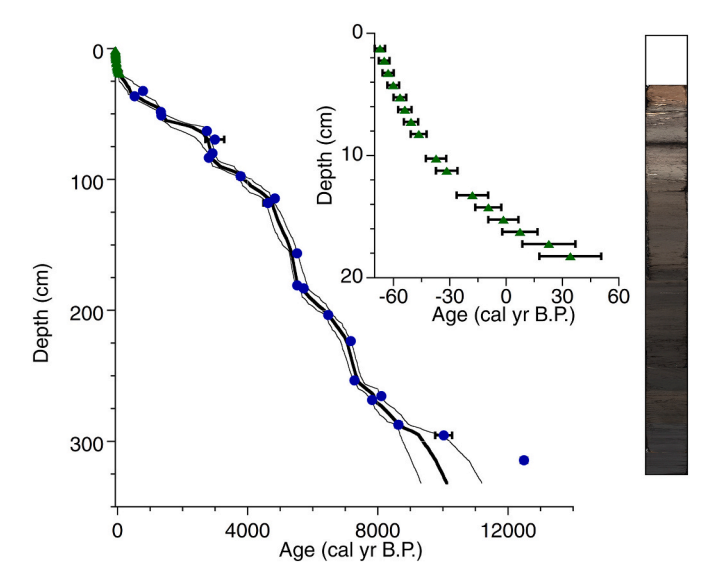


Fig. 3. Combined B-19 and C-19 age-depth model with 95% confidence intervals. ²¹⁰Pb dates (green diamonds) and radiocarbon dates (blue circles) are plotted with 2 sigma error bars. Inset-²¹⁰Pb dates. Core photos to the right. The uppermost 25 cm are missing from the core photos because these sediments were extruded in the field into bags. (For interpretation of the references to colour in this figure legend, the reader is referred to the web version of this article.)

periods of high lake level due to increased sediment transport distance. Alternatively, the radiocarbon date from 314.5 cm may be anomalously old due to the presence of inorganic carbon from the watershed, the socalled "hard water" effect that can appear in limestone catchments and particularly impact aquatic plants that use dissolved inorganic carbon (DIC) from the lake (Deevey et al., 1954). However, the paired dates of plants and charcoal from the top of the core (Table 2) suggest that the hard water effect is minimal (<250 years) in Yilong, although this could change through time. Despite possible underestimation of the basal age of the core, we adopt the Bacon age model estimations because it incorporates Bayesian statistics, which have been shown produce more realistic models than classical ones (Blaauw et al., 2018). Additionally, our analysis and interpretation focus on the upper 308 cm (9600 cal yr B. P.), the age estimations of which are unaffected by the lower 24 cm of core. With the exception of the base of the core, age uncertainty is usually less than ± 250 years.

4.2. Sediment composition

On the basis of changes in sediment composition (sedimentology, LOI, C/N, and Ti/Al), we divide the core into units (Fig. 4). Unit I is from 308 to 180 cm (9600 to 5500 cal yr B.P.), a transitional unit is from 180 to 112 cm (5500 to 4500 cal yr B.P.), Unit II is from 112 to 55 cm (4500 to 1500 cal yr B.P.), and Unit III is from 55 to 0 cm (1500 to -70 cal yr B. P.).

Unit I from 308 to 180 cm (9600 to 5500 cal yr B.P.) encompasses the base of the core which is dark brown fine-grained clay with extremely low carbonate content (<5%), moderately high organic matter content ($\sim15\%$), and high C/N ratio (<16). At 297 cm (9300 cal yr B.P.), there is an abrupt and irregular transition to dark gray silty clay. From 286 to 265 cm (8600 to 7900 cal yr B.P.), there an abrupt drop in C/N ratio (ranging between 12 and 16), a gradual increase in carbonate to 50%, and a gradual increase in organic matter to between 20 and 25%. Ti/Al ratio is relatively high. From 265 to 248 cm (7900 to 7300 cal yr B.P.), there is a decline in carbonate to around 20% and a slight increase in organic matter to between 25 and 30%. This is accompanied by an abrupt decline in Ti/Al ratio. At 248 cm (7300 cal yr B.P.), carbonate abruptly increases to between 35 and 40% and organic matter abruptly

decreases to between 20 and 25%. C/N ratio is slightly more variable, ranging between 22 and 15.

At 180 cm (5500 cal yr B.P.), there is an abrupt transition to lighter gray silty clay with frequent plant macrofossils. This is accompanied by transitions in other metrics of sediment composition that span from 180 and 112 cm (5500 to 4500 cal yr B.P.). Carbonate increases to \sim 60%, organic matter decreases to \sim 15%, and there is another rapid decline in Ti/Al ratio. C/N ratio is highly variable, ranging from 24 to 8.

Unit II spans from 112 to 55 cm (4500 to 1500 cal yr B.P.) and is marked by an abrupt transition to light gray fine-grained clay with intermittent plant macrofossils and broken shells. This is accompanied by another rapid increase in carbonate to between 80 and 85% and a further decline in organic matter to between 10 and 15%. C/N ratio gradually declines from 15 to 11 while Ti/Al ratio remains low and stable. This unit is briefly interrupted from 80 to 86 cm (3000 to 2900 cal yr B.P.) by a layer of plant material that begins abruptly and then gradually tapers off; it is marked by a brief peak in organic matter to 35% and a drop in C/N ratio to 4.

Unit III spans from 55 to 0 cm (1500 to -70 cal yr B.P.). There is a gradational contact to very fine-grained clay that was black when opened but turned red within 24 h of exposure to air. This transition is also marked by a layer of broken shells. Carbonate content rapidly declines from a peak of 85% to <15%. C/N ratio continues to gradually decline to around 4 with some brief increases to 9. Organic matter and carbonate content increase slightly in the uppermost 20 cm (60 cal yr B. P.) to 20% and 25%, respectively.

SEM images and XRD analysis from this study and XRD analysis by Yuan et al., 2021 identify that below 233 cm (7100 cal yr B.P.) siderite is mixed with calcite (Figs. S4 and 5). However, above this depth, there is an abrupt transition so that the only carbonate mineral present is calcite.

4.3. Isotope values

Given the extremely low carbonate content at the base of the core and that reliable isotope values could not be obtained, we confine our analysis and interpretations of isotope data to the upper 295 cm (9200 cal yr B.P.) (Fig. 4). With the exception of the lowermost 8 samples, the oxygen isotope record exhibits a pronounced trend toward less negative values moving from the base of the core to the top. This trend occurs in a mostly linear fashion albeit with three abrupt transitions at 7300, 4500, and 1500 cal yr B.P. Although inorganic carbon isotopes do not exhibit as pronounced a trend from the base to the top of the core as oxygen isotopes, in general, trends are similar to oxygen with the exception of the last 1500 cal yr B.P. Covariance between oxygen and carbon from 9200 to 1500 cal yr B.P. is high with an R² value of 0.80 and exhibits a positive linear trendline (Fig. 5). Covariance from 1500 cal yr B.P. to present-day is moderately high with an R² value of 0.47 and exhibits a negative linear trendline.

5. Discussion

5.1. Modern isotope calibration

The $\delta^{18}O$ value of authigenic calcite can be used to reconstruct the $\delta^{18}O$ value of the lake water during the time of formation when accounting for a predictable temperature dependent water-calcite transformation (Kim and O'Neil, 1997):

$$1000 ln\alpha(\text{Calcite} - \text{H}_2\text{O}) = 18.03 (10^3 T^{-1}) - 32.42$$
 (1)

To calculate the predicted $\delta^{18}O$ value of calcite precipitating in Yilong today, we used Eq. (1) where T=14.6 °C (the mean annual temperature of Kunming) and the lake water $\delta^{18}O$ value = -3.49% VSMOW from May 2019. It follows that calcite precipitating in isotopic equilibrium with the lake water should have a $\delta^{18}O$ value of -4.57% VPDB. The isotopic composition of the most recent surface sediments is

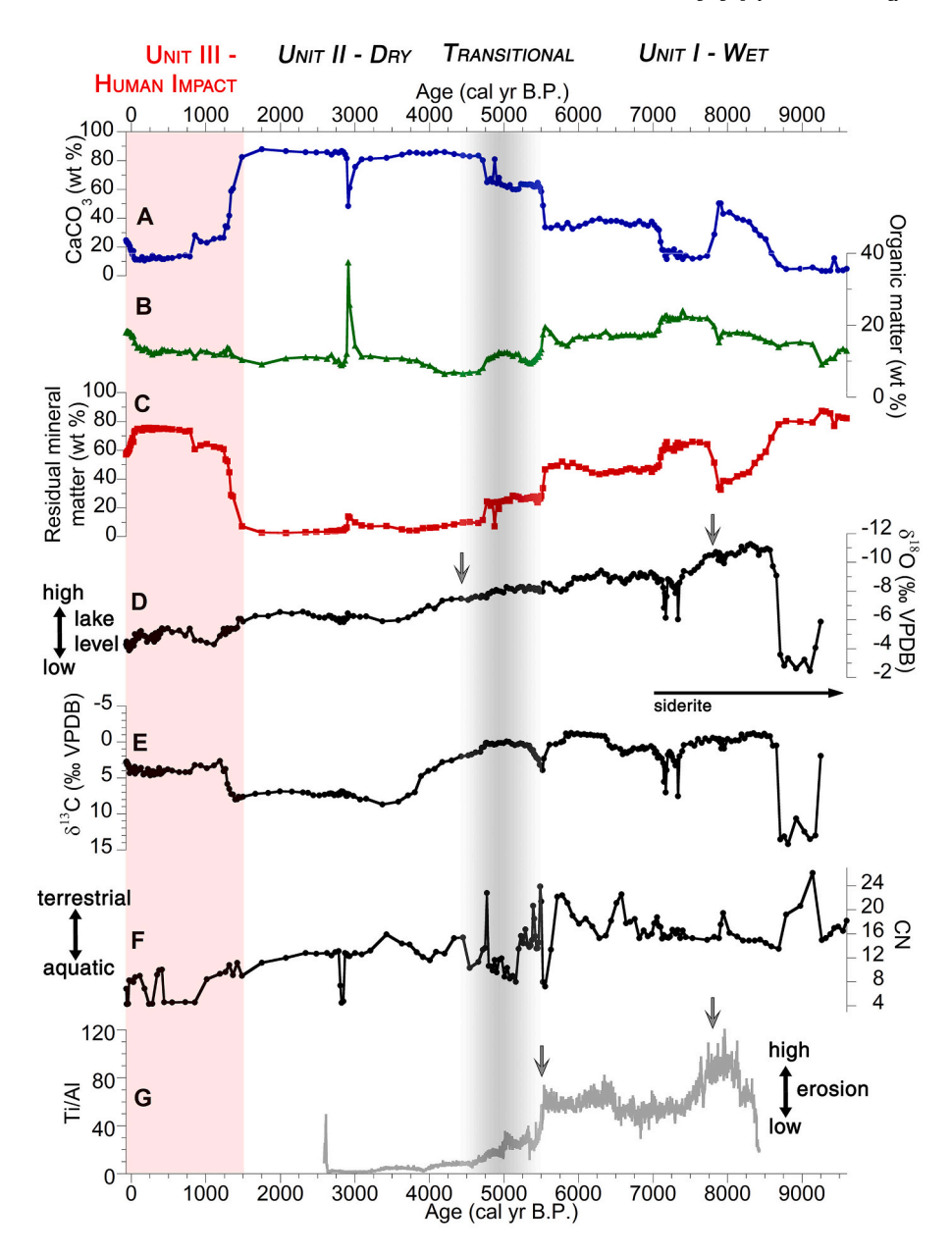


Fig. 4. A) B-19% carbonate estimated by LOI 1000 °C; B) B-19% organic matter estimated by LOI 550 °C; C) B-19% residual mineral matter; D) B-19 oxygen isotopes; E) B-19 carbon isotopes; F) B-19 carbon to nitrogen (C/N) ratios; G) A-19 Ti/Al ratio. Arrows mark decreases in either oxygen isotopes or Ti/Al ratio.

-4.28% VPDB, which is reasonably close given the uncertainties in these estimates. Our water isotope sample is a snapshot from only one year and likely changes from year to year. Also, we use the mean annual temperature of Kunming to estimate isotope values because we do not know the exact timing of calcite precipitation. Additionally, there may be offsets between air and water temperature. Nevertheless, we surmise that calcite is likely precipitating in equilibrium with the water given the general agreement between theoretical and actual isotope values. Estimating the δ^{18} O value of authigenic calcite that would precipitate from meteoric water alone (-9.9% VSMOW) yields a theoretical value of -12.1% VPBD, again demonstrating that evaporation effects on the lake water are substantial (Horton et al., 2016).

As in any lake that functions as a closed basin, precipitating calcite reflects variations in lake hydrology, driven by the combined changes in precipitation and evaporation. Water temperature also plays a role in influencing oxygen isotope values of calcite (-0.24%/1 °C) (Craig, 1965); however, this is offset by an opposing relationship between temperature and isotope values that arises from vapor to liquid

fractionation (+0.60%/1 °C) (Rozanski et al., 1993). The sum of these opposing influences (+0.36%/1 °C) means that while temperature can play a role in explaining calcite oxygen isotope values, it is minimal in comparison to the magnitude of changes that may be driven by precipitation and/or evaporation in a lake that functions as a closed basin.

The interpretation of oxygen isotope records from cave deposits from regions of Southeast Asia has been debated (Dayem et al., 2010; Liu et al., 2015; Rao et al., 2016), but we note that our interpretation of the influence of precipitation on lake water isotopic composition is not meant as a reconstruction of precipitation amounts, rather it is a reflection of the sum total of influences arising from upstream air mass processes. Less negative values are therefore reflective of a combination of less precipitation, a weaker ISM, and/or less rainout along the transport path; vice versa for more negative values. Similarly, given the strong influence that evaporation plays on influencing the isotopic composition of lake water in hydrologically sensitive basins, less negative values may also reflect greater water loss by evaporation driven by low humidity or enhanced solar radiation; vice versa for more negative

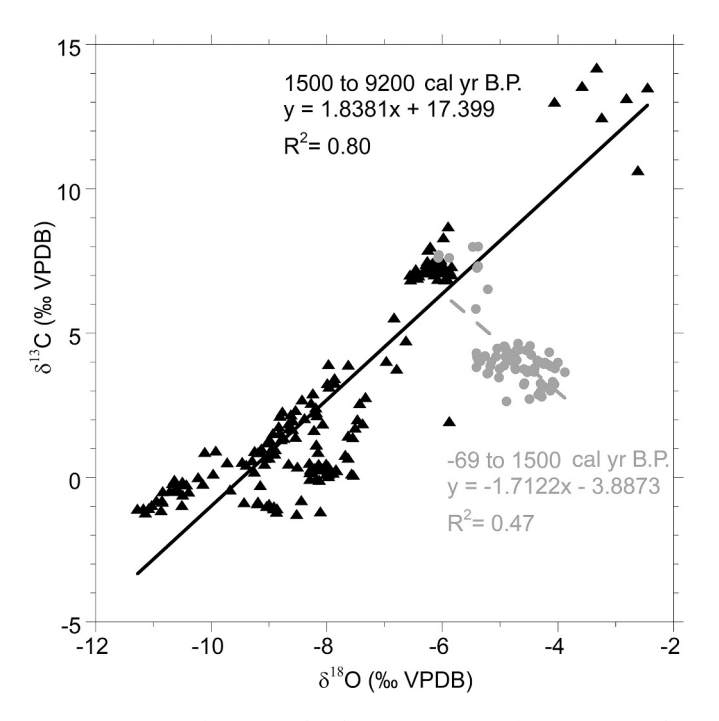


Fig. 5. Covariance of oxygen and carbon isotopes (B-19) for 1500-9200 cal yr B.P. in black triangles and for -69 to 1500 cal yr B.P. in gray circles.

values. While today Yilong may surficially outflow for part of the year, water flow is minimal and water isotope samples as well as theoretical calcite isotope values confirm that evaporation plays an important role in influencing water balance (Fig. 2). The strong covariance between oxygen and carbon isotopes throughout much of the Holocene (R $^2=0.80$) (Fig. 5) supports this supposition (Horton et al., 2016). Covariance between oxygen and carbon arises from changes in alkalinity, rate of $\rm CO_2$ exchange, and changes in primary productivity (Li and Ku, 1997). Particularly in the case of Yilong, increased evaporation leads to less negative $\delta^{18}\rm O$ values and increased $\rm CO_2$ evasion which also results in less negative $\delta^{13}\rm C$ values. In this way, we interpret the down-core record of Yilong isotopes to indicate precipitation-evaporation (P-E) conditions where less negative values suggest lower lake levels and vice versa for more negative values.

5.2. Erosional interpretive model

We primarily use scanning XRF data to examine relative downcore changes in Ti/Al ratio (Fig. 4G), indicative of high catchment erosion, and Ca/Al ratio (Fig. S6), indicative of low catchment erosion and high authigenic carbonate accumulation. In the presence of organic-rich sediment, the detection limit for Al on XRF scanners can be low, which may be a potential drawback of normalizing to Al (Löwemark et al., 2011). Incoherent to coherent scattering ratio (inc/coh) can account for changes in organic matter (Guyard et al., 2006). In general, inc/coh ratio is not inversely correlated to Al counts (Fig. S6), with the exception of one period around 3500 cal yr B.P. This suggests that our approach of normalizing to Al is not problematic.

We define two types of sediment composition: 1) low in weight percent carbonate with low Ca/Al ratio but high in residual mineral matter and high Ti/Al ratio due to erosion of sediment from the catchment; 2) low in residual mineral matter and low Ti/Al ratio but high in carbonate and high Ca/Al ratio when sediment composition is instead dominated by precipitation of carbonate from the water column. We interpret sediment type 1 to reflect high accumulation of material from catchment erosion. In Unit I this arises from increased monsoonal precipitation and the general trend from type 1 sediments to sediments more like type 2 suggests a reduction in this precipitation. Conversely, in

Unit II we interpret the dominance of sediment type 2 to reflect a lake environment with reduced catchment erosion. Despite the lack of XRF measurements from the A-19 surface core due to field extrusion to preserve the integrity of the stratigraphy, measurements of residual mineral matter concentration allow us to identify sediment type 1 in Unit III when human activities are the source of greater clastic input (Fig. 4A-C).

This erosional interpretive model is additionally supported by C/N ratio (Fig. 4F). A higher C/N ratio is indicative of increased terrestrial organic matter while a lower ratio suggests more aquatic organic matter (Meyers, 1994). When residual mineral matter and Ti/Al ratio are high, as in Unit I, C/N ratio is higher, suggesting that terrestrial carbon from the watershed contributed a larger proportion of carbon when erosion was higher. Conversely, when carbonate is high and Ti/Al ratios are low, as in Unit II, C/N ratio is lower, suggesting that terrestrial material contributions to organic matter accumulation were lower relative to aquatic primary productivity. Unit III is an exception to this trend, likely due to the influence of human activities such as land use change/agricultural activity, resultant erosion, and elevated nutrient delivery increasing primary productivity.

Since both Ti/Al ratio and $\delta^{18}O$ values reflect changes in precipitation regimes, we expect them to have similar trends, albeit with short-term differences. Ti/Al ratio is a proxy of erosion, but as discussed in Section 5.1, $\delta^{18}O$ values are a proxy of the balance between precipitation-evaporation, which has "memory" due to water residence time. Ti/Al ratios will therefore record short-term intense erosion events whereas $\delta^{18}O$ values are more likely to record longer-term trends in P-E balance. For example, this difference is apparent when Ti/Al ratios shift at 5500 cal yr B.P. but $\delta^{18}O$ values shift at 4500 cal yr B.P.

5.3. Trends prior to 1500 cal yr B.P

The long-term trend of oxygen isotope values and Ti/Al ratio is toward less negative values and a lower ratio, respectively (Fig. 4D, G). Lakes Xingyun, Qilu, and Yilong have similar oxygen isotope Holocene features (Fig. 6D-F) and this trend is further illustrated by the records from Qunf, Tham Doun Mai, and Heshang Caves (Fig. 6C, G-H). Notably, while both the lakes and caves have similar trends, the magnitude of change is different since the caves are primarily recording changes in precipitation while the lakes are recording changes in both precipitation and evaporation. The collection of proxies we have measured at Yilong lead us to conclude that Unit I represents wet conditions and Unit II represents drier conditions. On a first order, the transition between these two units is driven by the decline in Northern Hemisphere summer insolation (Fig. 6A) and a gradual southerly shift in the Intertropical Convergence Zone (ITCZ) as recorded in the Cariaco Basin (Fig. 6B). This interpretation is well-supported by other ISM records (e.g. Bird et al., 2014; Cai et al., 2012; Chen et al., 2014; Contreras-Rosales et al., 2014; Wang et al., 2017). Within the prominent Holocene-scale trend, there are several abrupt decreases at Yilong around 7900 (Ti/Al and δ^{18} O), 5500 (Ti/Al), and 4500 cal yr B.P. (δ^{18} O). We interpret these as periods when erosion (Ti/Al) or lake level (δ^{18} O) suddenly declined, reflecting sustained periods of less runoff or decreases in P-E balance, respectively.

The oxygen and carbon isotope values of the lowermost 8 samples from 9200 to 8700 cal yr B.P. (288–295 cm) and from 7300 to 7100 cal yr B.P. (233–248 cm) exhibit less negative values than the rest of the core (Fig. 4D, E). XRD analysis shows that siderite is present at 250 cm (Fig. S4) and a SEM image from 235 cm confirms that the increase in isotope values from 7300 to 7100 cal yr B.P. is coincident with siderite deposition (Fig. S5). Siderite generally forms at the sediment-water interface under strongly reducing conditions, often accompanied by methanogenic conditions and low sulfate concentrations (Leng et al., 2013). Given the reducing conditions necessary for siderite to form, methanogenesis by anaerobic bacteria can occur. High positive inorganic carbon isotope values in siderite have been observed (Leng et al., 2013) and are thought to be linked to the strong fractionation effect of

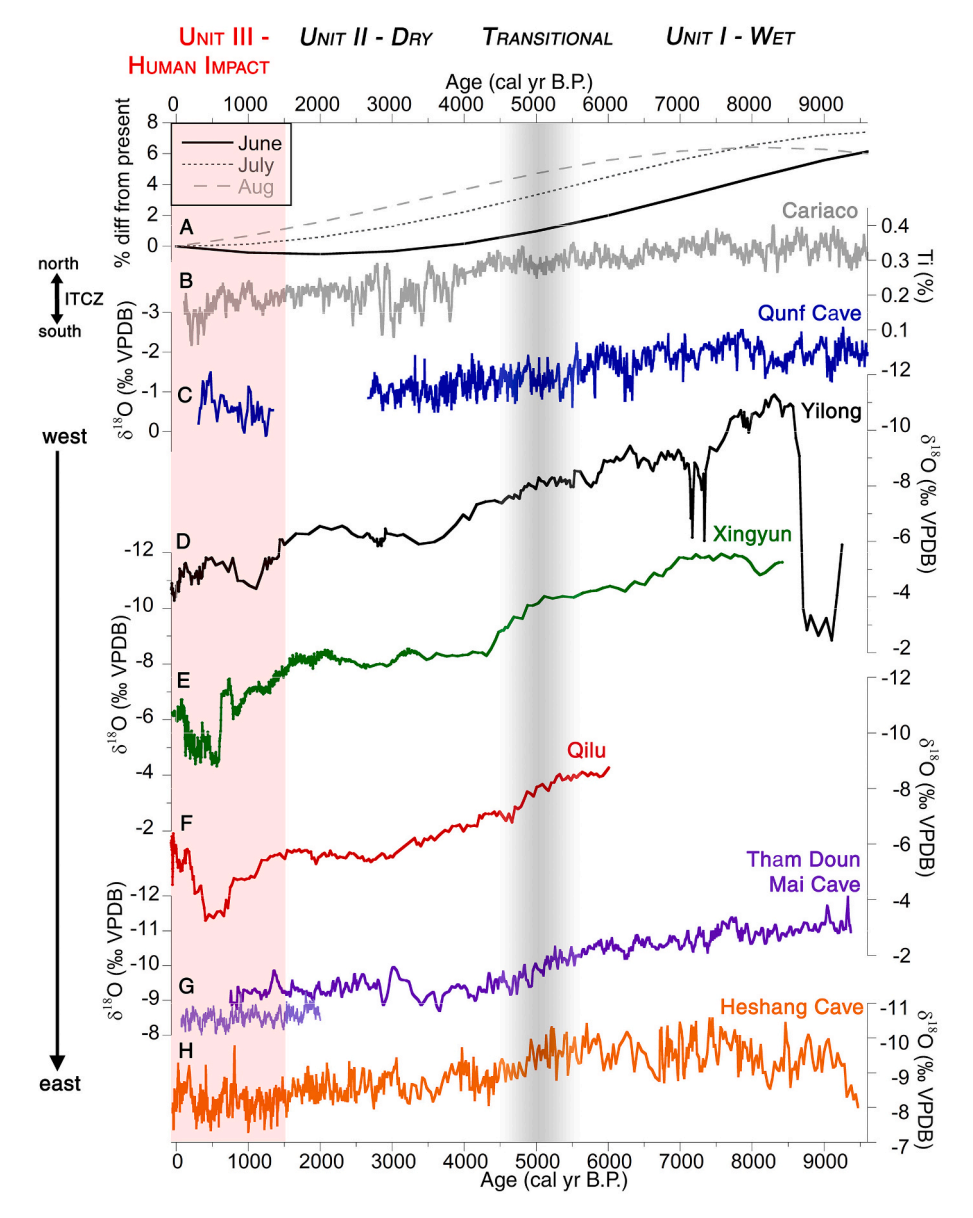


Fig. 6. A) June, July, August insolation as percent different from present-day (Laskar et al., 2004); B) Cariaco Basin percent Ti (Haug et al., 2001); C) Qunf Cave oxygen isotopes (Fleitmann et al., 2007); D) Yilong (B-19) oxygen isotopes; E) Xingyun oxygen isotopes (Hillman et al., 2017); F) Qilu oxygen isotopes (Hillman et al., 2020); G) Tham Doun Mai Cave oxygen isotopes (Griffiths et al., 2020; Wang et al., 2019); H) Heshang Cave oxygen isotopes (Hu et al., 2008).

methanogensis on enriching remaining bicarbonate in 13 C. Microbial-mediated changes in the DIC cycle can therefore likely account for the peaks in δ^{13} C values from 9200 to 8700 cal yr B.P. and from 7300 to 7100 cal yr B.P.

The magnitude of microbial mediated changes in oxygen isotopes due to siderite precipitation is unclear. Some earlier researchers suggested that microbially-mediated siderite formation can explain instances of extreme δ^{18} O values (-3.2%VPBD) (Mortimer and Coleman, 1997), but further examination of temperature-dependent fractionation across a wide range of temperatures and growth conditions suggests that this may be the case for only certain strains of bacteria (Zhang et al., 2001). The work of Zhang et al. (2001) generates a temperature sensitivity of -0.22%/1 °C, which has yielded reasonable lake water temperature estimates in some scenarios (Leng et al., 2013; Wittkop et al., 2014). However, more recent work suggests that microbially mediated siderite does not result in out of equilibrium precipitation, but that cation substitution of Ca, Mg, and Mn for Fe may constitute a significant source of uncertainty to isotopic fractionation factors (van Dijk et al.,

2019). As previously discussed, the role of temperature in influencing isotopic change at Yilong is likely small when compared with the magnitude of precipitation and/or evaporation effects. Indeed, Yuan et al. (2021) interpret the first excursion from 9200 to 8700 cal yr B.P. in Yilong to represent an intense drought, which is a distinct possibility. Given the limited information regarding siderite precipitation and its influence on $\delta^{18}{\rm O}$ values in P-E sensitive lakes, we refrain from interpreting this period as having paleoclimate significance but note the possibility.

Despite the presence of siderite below 235 cm (7100 cal yr B.P.) and questions regarding potential out of equilibrium precipitation, we interpret the gradual shift in $\delta^{18}\text{O}$ values at 7700 cal yr B.P. (±150 years) to reflect changes in climate, because of the similar shift in Ti/Al ratio after 7900 cal yr B.P. (±150 years) (Fig. 4G). Additionally, shifts in $\delta^{18}\text{O}$ values at Xingyun closely follow at 6900 cal yr B.P. (±400 years) (Fig. 6E), and because age control through this section of Xingyun is relatively weak, these events may have occurred close in time to one another. Alternatively, because Yilong likely has a shorter water

residence compared to Xingyun given its smaller size (Table 1), it may have responded more quickly to a change in P-E balance.

Another abrupt decline in Ti/Al ratio at around 5500 cal yr B.P. (Fig. 4G) is roughly coincident with shifts to less negative values in oxygen isotopes at nearby Xingyun (5500 cal yr B.P. \pm 350 years) (Hillman et al., 2017) and Qilu (5200 cal yr B.P. \pm 300 years) (Hillman et al., 2020) lakes (Fig. 6E-F). Yilong has a similar magnitude shift in oxygen isotopes (1.5‰) that begins $\sim\!1000$ years later at 4500 cal yr B.P. (\pm 250 years) (Fig. 4D). The strong positive response of the inorganic carbon isotopes (6.7‰ VPDB) that also begins at 4500 cal yr B.P. (Fig. 4E) supports our assertion that a decline in lake level is responsible for the Yilong isotope excursion, since a net loss of CO₂ to the atmosphere from evaporation and/or vertical mixing within the water column can lead to increases in δ^{13} C values (Li and Ku, 1997).

The lag in isotopic response at Yilong may be due to differences in water residence time or lake sensitivity. Substantial differences in catchment area to lake volume (Table 1) may result in a hydrologic response time lag causing each lake to have a different sensitivity. Previous work has shown that lake morphometry, groundwater throughflow, and water residence time characteristics can account for inconsistent responses amongst adjacent closed basin lakes to the same hydrologic forcing (Steinman et al., 2010). For these lakes in Yunnan, lake morphometry is well-constrained, but other variables (e.g., groundwater throughflow, water residence time) are not, precluding us from using a hydrologic isotope mass-balance model to quantify response and residence time. It is also possible that some of these differences in timing may be due to chronological uncertainty since, when considering age model uncertainties, the declines in lake level at Xingyun, Qilu, and Yilong overlap.

Nonetheless, we conclude that between 5500 and 4500 cal yr B.P., a combination of decreases in precipitation and/or increases in evaporation resulted in increasingly arid conditions which manifested at lakes throughout Yunnan as a transitional period from wet to dry conditions. Lake Dian, further to the north, also shows indications of aridity at 4000 cal yr B.P., with increasing accumulation of coarse-grained sand (Yan et al., 2020). In other Yunnan lakes, this is observed in palynological records (Song et al., 2012; Xiao et al., 2017; Yang et al., 2016). A number of records from the Tibetan Plateau also show evidence of aridity between 5000 and 4000 cal yr B.P. including: oxygen isotopes of lakes (Gasse et al., 1996; Morrill et al., 2006), hydrogen isotopes of a lake (Hou et al., 2017), grain size variability of a lake (Bird et al., 2014), and oxygen isotopes from caves (Berkelhammer et al., 2012; Cai et al., 2012). Both oxygen and carbon isotopes from Tham Doun Mai Cave in Laos also display an abrupt arid period starting at 5000 cal yr B.P. (Griffiths et al., 2020) (Fig. 6G). We therefore suggest that gradual climate forcing cannot explain our observations at Xingyun, Qilu, and Yilong and that changes in Pacific and/or Indian Ocean dynamics are a likely possibility; this will be further explored in Section 5.4.

Similar to both Xingyun and Qilu, Yilong $\delta^{18}O$ values from 3500 to 1500 cal yr B.P. are stable (average $=-6.16\%\pm0.2$) in comparison to previous time periods despite continued ISM weakening. Previously, we had suggested that the unique bathymetry of Xingyun permitted isotope values to stay remarkably stable (Hillman et al., 2017). While the period of stability is longest at Xingyun, its presence at both Qilu and Yilong suggests that bathymetry may not wholly account for this apparent stability. This is unexpected given that continued declines in ISM strength could be used to predict less monsoon precipitation leading to a progressive increase in $\delta^{18}O$ values. The lack of a millennial scale trend in $\delta^{18}O$ values may instead be caused by a decline in evaporation. However, with decreased ISM intensity, cloud cover is expected to decrease and result in more solar radiation driving greater evaporation.

From 9200 to 1500 cal yr B.P., the magnitude of isotopic change in cave records from Southeastern Asia and China is 2 or 3‰, (Tham Doun Mai (Griffiths et al., 2020), Heshang (Hu et al., 2008), Dongge (Wang et al., 2005)), which we assume represents the total change in oxygen isotopic composition of monsoonal precipitation arising from upstream

airmass processes. Over the same period, the isotopic change at Yilong is 7‰. Assuming that temperature plays a minimal role in accounting for this change, 4 or 5‰ of isotopic modification at Yilong must be driven by evaporation. As detailed in Gat's, 1995 equations for terminal lakes at hydrological and isotopic steady state, one of the principal controls on the degree of isotopic enrichment is ambient humidity (Gat, 1995):

$$\Delta \delta = (1 - h)(\varepsilon^* + C_k) \tag{2}$$

where h= humidity, $\varepsilon^*=$ the equilibrium isotope separation factor, and $C_k=$ the kinetic constant. C_k has been experimentally determined to be 15% for oxygen (Gat, 1995). We calculated ε^* as:

$$\varepsilon^* = 1000^*(1 - \alpha^*) \tag{3}$$

where α^* is the reciprocal of the equilibrium isotopic fractionation factor α . α was calculated based on the equation (Horita and Wesolowski, 1994):

$$ln\alpha = 0.35041 \frac{10^6}{T^3} - 1.6664 \frac{10^3}{T^2} + 6.7123 \frac{1}{T} - 7.685 \times 10^{-3}$$
 (4)

where T = temperature of the lake water.

Assuming a lake water temperature of $14.5\,^{\circ}\mathrm{C}$ (similar to today), that the lake was in an isotopic steady state, and that changes in the isotopic composition of precipitation at Yilong were similar to changes at monsoonal cave records, this yields an estimate that the early Holocene was roughly 10 to 15% more humid than 1500 cal yr B.P. While there are many assumptions built into this estimate, these equations generate constraints on potential conditions during the early Holocene. To further explore this Holocene scale change, and other features of the down-core oxygen isotopes further, we now examine potential driving mechanisms.

5.4. Potential mechanisms for Holocene shifts

The first abrupt transition at 7900 cal yr B.P. (Ti/Al ratio) and 7700 cal yr B.P. (δ^{18} O values) is close in timing to the North Atlantic's 8200 cal yr B.P. (8.2) event. This event occurred when ice-rafted debris in the North Atlantic resulted in a southerly shift of the ITCZ and the monsoonal rain belt (Fig. 6B, C) (Bond et al., 2001; Fleitmann et al., 2003; Fleitmann et al., 2007; Haug et al., 2001). The 8.2 event was short-lived whereas the decline in Ti/Al ratio and δ^{18} O values at Yilong are a protracted shift in mean-state. However, we cannot rule out the possibility that this was triggered by the 8.2 event in the North Atlantic.

A gradual southerly shift in the ITCZ after a maximum between ~9000 and 7000 cal yr B.P. driven by declining Northern Hemisphere summer insolation is recorded in the Cariaco Basin (Haug et al., 2001) (Fig. 6B). A more southerly position of the ITCZ enhances El Niño Southern Oscillation (ENSO) and Indian Ocean Dipole (IOD) events (Freitas et al., 2017), whereas a more northerly position attenuates ENSO (Koutavas et al., 2006). ENSO events tend to weaken the ISM (Kumar et al., 2006), but the magnitude and sign of precipitation anomalies varies spatially due to different ENSO types (Yuan and Yang, 2012). Positive precipitation anomalies in the transition zone of Southeast Asia can result from eastern Pacific (EP) events driven by stronger winds over the Bay of Bengal whereas negative anomalies result from central Pacific (CP) events caused by a shift to more northerly winds (Hernandez et al., 2015). Some records find evidence for a predominance of CP events relative to EP events around 7000 cal yr B.P. (Carre et al., 2014) although the timing of the initiation of these conditions is unknown. Additionally, although results are not consistent amongst all paleo ENSO reconstructions, weak ENSO variability in the early Holocene is a common feature of many (as reviewed in Lu et al., 2018), and consequently it is less likely that ENSO is an important mechanism in driving our inferred lake level decline at ~7900 to 7700 cal yr B.P.

We consider that the IOD may play an important role. The expression of modern-day IOD events in southwestern China is opposite to other

monsoon regions (e.g., India, eastern China) such that positive IOD events result in negative precipitation anomalies driven by easterly winds which weaken the supply of moisture from the Bay of Bengal (Cao et al., 2014; Liu et al., 2018; Ratna et al., 2021). Previous research from the Mentawai Islands has found evidence for a positive IOD mean-state prior to 6800 cal yr B.P. (Abram et al., 2009). We acknowledge that there is some uncertainty in invoking this mechanism and note that the status of the IOD in the early Holocene and the relationship between mean-state and annual changes in the IOD need additional study.

There is marked change throughout regions impacted by both the ISM and EASM from 5500 to 4500 cal yr B.P., the transition period from wet to dry in the Yilong record. Notably, the ITCZ shifts abruptly southward around 4000 cal yr B.P. (Haug et al., 2001) and may explain the presence of such a transition in cave records such as Tham Doun Mai (Griffiths et al., 2020) or Heshang (Hu et al., 2008) (Fig. 6G, H). However, as discussed in the Section 5.3, the magnitude of isotopic change recorded in Yilong, Xingyun, and Qilu is larger than that of the cave records, suggesting that evaporation is a prominent driver. We suggest ITCZ amplification of Pacific and Indian ocean dynamics plays a key role in controlling periods of aridity in Southeastern Asia. Also important are the differential impacts of ENSO events based on the proportion of EP relative CP events during the middle Holocene. Modeling suggests that CP events were more frequent and stronger in the middle Holocene (Karamperidou et al., 2015), but many paleo studies show evidence for widespread reduced ENSO variability from 5000 to 3000 cal yr B.P. (Grothe et al., 2019). After 4000 cal yr B.P., enhanced ENSO variability is a feature of many sediment records (as summarized in Lu et al., 2018), particularly those in the EP region.

The difference in timing between changes in ENSO frequency and strength and our inferred period of aridity makes it unlikely that this forcing fully explains our findings. However, given that modern-day ENSO interacts with and drives variations in IOD (Abram et al., 2020), these two mechanisms may be linked. Support for this idea comes from a recent modeling study that links the weakening of the West African Monsoon around 5000 cal yr B.P. with an eastward shift of the Walker circulation and the initiation of cooler SSTs in the western Pacific (El Niño-like) and eastern Indian Ocean (positive IOD) (Griffiths et al., 2020; Pausata et al., 2017). A Holocene length reconstruction of the IOD finds evidence for a persistently positive mean-state from 5500 to 4300 cal yr B.P. (Abram et al., 2009), making these connections plausible. Our results, recent reviews, and modeling studies suggest that Pacific and Indian Ocean dynamics are intertwined with the ISM and shifting location of the ITCZ. However, further studies that examine and clarify the relative importance of these mechanisms throughout the Holocene are needed.

An unusual feature of the Yunnan lake records are isotope values that are stable from 3500 to 1500 cal yr B.P. Such stability is also present in hydrogen isotopes of n-alkanes from nearby Lugu Lake (Zhao et al., 2021). However, cave records from eastern China (Fig. 6H) (e.g., Hu et al., 2008; Wang et al., 2008; Yang et al., 2019) show continued isotopic enrichment, indicating a progressive waning of the EASM. A variety of records from the ISM region, including the Tibetan Plateau (Cai et al., 2012; Hou et al., 2017), Oman (Fig. 6C) (Fleitmann et al., 2007), and Indian lake records (as summarized in Misra et al., 2019) display profound aridity. Given that reorganization of Indian Ocean dynamics occurred between 5500 and 4300 cal yr B.P. (Abram et al., 2009), quiescence after 4000 cal yr B.P. may explain the period of P-E stability in Yunnan. However, this is not a satisfactory explanation since Indian Ocean dynamics are expected to influence other ISM regions. It is important to consider that the modern-day expression of ENSO and IOD events in southwestern China, Myanmar, and northeastern India have opposite sign anomalies to other regions, making these regions important for further hypothesis testing.

5.5. Trends after 1500 cal yr B.P

The layer of plant material in Yilong sediments from 3000 to 2900 cal yr B.P. with low C/N values suggests a sudden increase in aquatic organic matter deposition (Fig. 4F). This may suggest a low lake level stand although oxygen isotopes through this interval remain mostly unchanged; the event may have been too transient to be recorded in the oxygen isotopes. Alternatively, palynological analysis of sediment at Dian identified significant human impact on the vegetation of the surrounding catchment at 2400 cal yr B.P. (Xiao et al., 2020). Hence, this layer may signify the beginning of anthropogenic disturbance in the form of deforestation within the Yilong catchment that resulted in nutrient in wash and higher primary productivity.

At 1500 cal yr B.P., the positive oxygen isotope shift at Yilong of 1.8‰ is coincident with an oxygen isotope shift at both Xingyun and Qilu lakes (Fig. 6D-F), which has previously been established as a time when anthropogenic manipulation of lake hydrology in Yunnan became widespread (Hillman et al., 2017; Hillman et al., 2020). At all three lakes this shift in isotopes is also coincident with the deposition of red, very fine-grained clay. The deposition of this red clay unit has previously been linked to intense catchment-wide land use change and erosion (Brenner et al., 1991; Hillman et al., 2019; Hillman et al., 2014; Hodell et al., 1999; Wu et al., 2014).

We interpret the 1.8% positive oxygen isotope shift at Yilong at 1500 cal yr B.P. to be the result of human hydrologic manipulation, specifically a combination of water withdrawal for irrigation and/or stream diversion. At Xingyun, historical records support this interpretation (Hillman et al., 2014). While we have not identified historical records to support this at Yilong, we still consider anthropogenic manipulation to be the most likely explanation due to support from multiple proxies (e.g., sedimentology, sediment composition) and the lack of a clear climate driver. Nearby Tham Doun Mai Cave does not display prolonged drought at 1500 cal yr B.P. (Fig. 6G) (Griffiths et al., 2020; Wang et al., 2019). There are also numerous other lake sediment records from Yunnan that document that human activity became the dominant driver of environmental change within the last 2000 cal yr B. P. (Hillman et al., 2019; Xiao et al., 2017; Xiao et al., 2015; Xiao et al., 2020).

Also, strikingly similar to both Xingyun and Qilu, Yilong exhibits a large magnitude (4.5%) and rapid (~200 years) negative shift in inorganic carbon isotopes at 1300 cal yr B.P. (Fig. 4E). The lack of strong covariance through this period (Fig. 5) does not necessarily indicate that Yilong behaved as an open basin particularly since values are still enriched relative to what would be expected if calcite were precipitating from meteoric water unimpacted by evaporation (Horton et al., 2016). A stable climate (Horton et al., 2016) and/or stable lake levels (Li and Ku, 1997) have been suggested as possible reasons for why closed basin lakes may not exhibit covariant trends. However, in the case of Yilong, we suggest that profound human disturbance perturbing the carbon cycle of the lake related to population and agricultural expansion accounts for the lack of covariance. One possibility is that if the lake were pushed toward a eutrophic state, as low C/N ratio (Fig. 4F) and therefore high primary productivity indicate, oxidation of ¹³C-depleted organic matter, and/or methanogenesis may have changed the composition of the DIC pool (Hollander and Smith, 2001).

A sustained period of less negative oxygen isotope values at Yilong occurs from 1100 to 800 cal yr B.P., which coincides with the Medieval Climate Anomaly (MCA) (ca. 1000 to 700 cal yr B.P.). Tham Doun Mai Cave does not display any prominent wet or dry periods during the MCA (Fig. 6G) (Wang et al., 2019), while records from mid-latitude China (around >30° N) are dominated by wet conditions (Chen et al., 2015). Most records from India also suggest wetter conditions although greater aridity is noted further to the east (Dixit and Tandon, 2016). In a landscape that has been profoundly impacted by humans, it is difficult to extract a natural climate signal, however given the lack of a clear spatial pattern indicating dry conditions during the MCA, we conclude that this

period suggests continued freshwater resource use for activities such as agriculture. However, relative to Xingyun and Qilu, variability in oxygen isotopes within the last 1500 cal yr B.P. at Yilong is dampened (Fig. 6D-F). There are no abrupt shifts as there are at Xingyun (e.g., 800 or 600 cal yr B.P.) or Qilu (e.g., 600 cal yr B.P.) and century-scale trends are less prominent. Hence, we suggest that while human impacts are present at Yilong, the lake hydrologic balance was less intensively managed. This highlights the significant spatial variability that can occur with human activities and underscores the importance of generating multiple records within a region to better characterize anthropogenic impacts as population expands and the intensity of human manipulation of hydrology increases.

Lastly, beginning around 50 cal yr B.P., there is a trend in Yilong oxygen isotopes toward less negative values, some of the least negative values of the entire record. This strongly suggests that present-day lake levels are low relative to the rest of the Holocene, arising from a combination of a fairly weak ISM as well as human modification and water use. Satellite imagery confirms that lake levels have varied substantially within the last few decades which has an impact on the lake hydrologic budget (Fig. S1).

6. Conclusion

Modern measurements of precipitation and lake water isotopes as well as down-core isotopic measurements of authigenic calcite indicate that Yilong Lake is hydrologically sensitive and strongly influenced by the balance between precipitation and evaporation. Sediment composition, oxygen and carbon isotopes of calcite, and Ti/Al ratio over the past 9200 cal yr B.P. reveal the declining strength of the ISM over the Holocene. Yilong and nearby Xingyun and Qilu lakes have remarkably similar Holocene and centennial-scale oxygen isotope trends, suggesting they respond to the same factors driving changes in regional P-E balance over a range of timescales. The gradual Holocene decline at Yilong is driven by a southward shift in the ITCZ, potentially enhancing ENSO and IOD events and interactions. We suggest this leads to abrupt decreases in precipitation and/or enhanced evaporation at ~7900, 5500, and 4500 cal yr B.P. The Yilong, Xingyun, and Qilu records thereby demonstrate characteristic responses of lake hydrological balance in the ISM region to orbital-scale monsoon forcing; however, they also highlight regional distinctiveness in Yunnan on centennial and multidecadal-scales. These results suggest that despite well-established general monsoon trends through the Holocene, continued research on finer timescales is still necessary and fruitful.

In general, previous studies have documented changes to vegetation around Yunnan lake catchments occurring between 4000 and 2000 cal yr B.P. (Shen et al., 2006; Xiao et al., 2015; Xiao et al., 2017; Xiao et al., 2020). This study shows that in many cases, this is followed at 1500 cal yr B.P. by increased rates of erosion from land use changes and high oxygen isotope variability from human manipulation of water balance. This ultimately demonstrates the gradual intensification of pre-Industrial anthropogenic impacts to the landscape. However, we also show that the manifestation of these impacts at Yilong is muted compared to nearby lakes Xingyun and Qilu, demonstrating that each lake and its catchment's exploitation is unique and records climate and landscape changes at slightly different temporal resolutions. This record emphasizes the complexity of disentangling human impacts from natural climate change and the continued need for additional paleoclimate archives in order to discern changes in the ISM on centennial and decadal timescales.

Data availability

Datasets related to this article can be found at https://data.mendele y.com/datasets/87tzm7frmp/2, an open-source online data repository hosted at Mendeley Data.

Declaration of Competing Interest

None.

Acknowledgements

This work was financially supported by a United States NSF-EAR Geomorphology and Land Use Dynamics grant to Aubrey Hillman (#1648634 and #2120366) and Daniel Bain and Mark Abbott (#1648772), and the National Natural Science Foundation of China (#41991251). We thank David Dettman for the analysis of stable isotopes, Jay Goodin and Ryan Hood for assistance with lab work, and Don Rodbell and Matthew Monan for use of the XRD at Union College. We thank two anonymous reviewers for their helpful comments and suggestions.

Appendix A. Supplementary data

Supplementary data to this article can be found online at https://doi. org/10.1016/j.palaeo.2022.111148.

References

- Abram, N.J., McGregor, H.V., Gagan, M.K., Hantoro, W.S., Suwargadi, B.W., 2009. Oscillations in the southern extent of the Indo-Pacific warm Pool during the mid-Holocene. Quat. Sci. Rev. 28, 2794–2803.
- Abram, N.J., Hargreaves, J.A., Wright, N.M., Thirumalai, K., Ummenhofer, C.C., England, M.H., 2020. Palaeoclimate perspectives on the Indian Ocean Dipole. Quat. Sci. Rev. 237.
- Araguas-Araguas, L., Froehlich, K., Rozanski, K., 1998. Stable isotope composition of precipitation over Southeast Asia. J. Geophys. Res. 103, 28721–28742.
- Bai, J., Cui, B., Chen, B., Zhang, K., Deng, W., Gao, H., Xiao, R., 2011. Spatial distribution and ecological risk assessment of heavy metals in surface sediments from a typical plateau lake wetland, China. Ecol. Model. 222, 301–306.
- Berkelhammer, M., Sinha, A., Stott, L.D., Cheng, H., Pausata, F.S.R., Yoshimura, K., 2012. An Abrupt Shift in the Indian Monsoon 4000 Years Ago. American Geophysical Union
- Binford, M.W., 1990. Calculation and uncertainty analysis of ²¹⁰Pb dates for PIRLA project lake sediment cores. J. Paleolimnol. 3, 253–267.
- Bird, B.W., Polisar, P.J., Lei, Y., Thompson, L.G., Yao, T., Finney, B.P., Bain, D.J., Pompeani, D.P., Steinman, B.A., 2014. A Tibetan lake sediment record of Holocene Indian summer monsoon variability. Earth Planet. Sci. Lett. 399, 92–102.
- Blaauw, M., Christen, J.A., 2011. Flexible paleoclimate age-depth models using an autoregressive gamma process. Bayesian Anal. 6, 457–474.
- Blaauw, M., Christen, J.A., Bennet, K.D., Reimer, P.J., 2018. Double the dates and go for Bayes – Impacts of model choice, dating density and quality on chronologies. Quat. Sci. Rev. 188, 58–66.
- Bond, G., Kromer, B., Beer, J., Muscheler, R., Evans, M.N., Showers, W., Hoffmann, S., Lotti-Bond, R., Hajdas, I., Bonani, G., 2001. Persistent solar influence on North Atlantic climate during the Holocene. Science 294, 2130–2136.
- Brenner, M., Dorsey, K., Xueliang, S., Zuguan, W., Ruihua, L., Binford, M.W., Whitmore, T.J., Moore, A.M., 1991. Paleolimnology of Qilu Hu, Yunnan Province, China. Hydrobiologia 214, 333–340.
- Bureau of Geology and Mineral Resources of Yunnan Province, 1990. Regional Geology of Yunnan Province. Geological Publishing House, Beijing.
- Cai, Y., Zhang, H., Cheng, H., An, Z., Lawrence Edwards, R., Wang, X., Tan, L., Liang, F., Wang, J., Kelly, M., 2012. The Holocene Indian monsoon variability over the southern Tibetan Plateau and its teleconnections. Earth Planet. Sci. Lett. 335-336, 135-144.
- Cao, J., Yao, P., Wang, L., Liu, K., 2014. Summer rainfall variability in low-latitude Highlands of China and Subtropical Indian Ocean Dipole. J. Clim. 27, 880–892.
- Carre, M., Sachs, J.P., Purca, S., Schaner, A.J., Braconnot, P., Falcon, R.A., Julien, M., Lavallee, D., 2014. Holocene history of ENSO variance and asymmetry in the eastern tropical Pacific. Science 345, 1045–1048.
- Chen, F., Chen, X., Chen, J., Zhou, A., Wu, D., Tang, L., Zhang, X., Huang, X., Yu, J., 2014. Holocene vegetation history, precipitation changes and Indian Summer Monsoon evolution documented from sediments of Xingyun Lake, south-west China. J. Ouat. Sci. 29. 661–674.
- Chen, J., Chen, F., Feng, S., Huang, W., Liu, J., Zhou, A., 2015. Hydroclimatic changes in China and surroundings during the Medieval Climate Anomaly and Little Ice Age: spatial patterns and possible mechanisms. Ouat. Sci. Rev. 107, 98–111.
- Cheng, H., Sinha, A., Wang, X., Cruz, F.W., Edwards, R.L., 2012. The Global Paleomonsoon as seen through speleothem records from Asia and the Americas. Clim. Dyn. 39, 1045–1062.
- Contreras-Rosales, L.A., Jennerjahn, T., Tharammal, T., Meyer, V., Lückge, A., Paul, A., Schefuß, E., 2014. Evolution of the Indian Summer Monsoon and terrestrial vegetation in the Bengal region during the past 18 ka. Quat. Sci. Rev. 102, 133–148.
- Craig, H., 1965. The measurement of oxygen isotope palaeotemperatures. In: Tongiorgi, E. (Ed.), Stable Isotopes in Oceanographic Studies and

- Palaeotemperatures. Consiglio Nazionale delle Ricerche Laboratorio di Geologia Nucleare. Pisa.
- Dayem, K.E., Molnar, P., Battisti, D.S., Roe, G.H., 2010. Lessons learned from oxygen isotopes in modern precipitation applied to interpretation of speleothem records of paleoclimate from eastern Asia. Earth Planet. Sci. Lett. 295, 219–230.
- Dean, W.E., 1974. Determination of carbonate and organic matter in calcareous sediments and sedimentary rocks by loss on ignition: comparison with other methods. J. Sediment. Petrol. 44, 242–248.
- Deevey, E.S., Gross, M.S., Hutchinson, G., Kraybill, H.L., 1954. The natural C14 contents of materials from hard-water lakes. Geology 40, 285–288.
- Dixit, Y., Tandon, S.K., 2016. Hydroclimatic variability on the Indian subcontinent in the past millennium: review and assessment. Earth Sci. Rev. 161, 1–15.
- Fleitmann, D., Burns, S., Mudelsee, M., Neff, U., Kramers, J., Mangini, A., Matter, A., 2003. Holocene forcing of the Indian Monsoon recorded in a stalagmite from Southern Oman. Science 300, 1737–1739.
- Fleitmann, D., Burns, S.J., Mangini, A., Mudelsee, M., Kramers, J., Villa, I., Neff, U., Al-Subbary, A.A., Buettner, A., Hippler, D., Matter, A., 2007. Holocene ITCZ and Indian monsoon dynamics recorded in stalagmites from Oman and Yemen (Socotra). Quat. Sci. Rev. 26, 170–188.
- Freitas, A.C.V., Aimola, L., Ambrizzi, T., Prestelo de Oliveira, C., 2017. Extreme intertropical convergence zone shifts over Southern Maritime Continent. Atmos. Sci. Lett. 18, 2–10.
- Gasse, F., Fontes, F.Ch., Van Campo, E., Wei, K., 1996. Holocene environmental changes in Bangong Co basin (Western Tibet). Part 4: discussion and conclusions. Palaeogeogr. Palaeoclimatol. Palaeoecol. 120, 79–92.
- Gat, J.R., 1995. Stable isotopes of fresh and saline lakes. In: Lerman, A., Imboden, D.M., Gat, J.R. (Eds.), Physics and Chemistry of Lakes. Springer, Berlin, pp. 139–165.
- Griffiths, M.L., Johnson, K.R., Pausata, F.S.R., White, J.C., Henderson, G.M., Wood, C.T., Yang, H., Ersek, V., Conrad, C., Sekhon, N., 2020. End of Green Sahara amplified mid- to late Holocene megadroughts in mainland Southeast Asia. Nat. Commun. 11, 4204
- Grothe, P.R., Cobb, K.M., Liguori, G., Di Lorenzo, E., Capotondi, A., Lu, Y., Edwards, R.L., Southon, J.R., Santos, G.M., Deocampo, D.M., Lynch-Stieglitz, J., Chen, T., Sayani, H., Thompson, D.M., Conroy, J.L., Moore, A.L., Townsend, K., Hagos, M., O'Connor, G., Toth, L.T., 2019. Enhanced El Niño–Southern oscillation variability in recent decades. Geophys. Res. Lett. 46 e2019GL083906.
- Gupta, A.K., Anderson, D.M., Overpeck, J.T., 2002. Abrupt changes in the Asian southwest monsoon during the Holocene and their links to the North Atlantic Ocean. Nature 421.
- Guyard, H., Chapron, E., St-Onge, G., Anselmetti, F.S., Arnaud, F., Magand, O., Francus, P., Mélières, M.-A., 2006. High-altitude varve records of abrupt environmental changes and mining activity over the last 4000 years in the Western French Alps (Lake Bramant, Grandes Rousses Massif). Ouat. Sci. Rev. 26, 2644–2660.
- Haug, G.H., Hughen, K.A., Peterson, L.C., Sigman, D.M., Röhl, U., 2001. Southward migration of the intertropical convergence zone through the Holocene. Science 293, 1304–1308.
- Hernandez, M., Ummenhofer, C.C., Anchukaitis, K.J., 2015. Multi-scale drought and ocean–atmosphere variability in monsoon Asia. Environ. Res. Lett. 10, 074010.
- Hillman, A.L., Yu, J., Abbott, M.B., Cooke, C.A., Bain, D.J., Steinman, B.A., 2014. Rapid environmental change during dynastic transitions in Yunnan Province, China. Quat. Sci. Rev. 98, 24–32.
- Hillman, A.L., Abbott, M.B., Finkenbinder, M.S., Yu, J., 2017. An 8,600 year lacustrine record of summer monsoon variability from Yunnan, China. Quat. Sci. Rev. 174, 120–132.
- Hillman, A.L., Yao, A., Abbott, M.B., Bain, D.J., 2019. Two Millennia of Anthropogenic Landscape Modification and Nutrient Loading at Dian Lake, Yunnan Province, China. The Holocene.
- Hillman, A.L., O'Quinn, R.F., Abbott, M.B., Bain, D.J., 2020. A Holocene history of the Indian monsoon from Qilu Lake, southwestern China. Quat. Sci. Rev. 227, 106051.
- Hodell, D.A., Brenner, M., Kanfoush, S.L., Curtis, J.H., Stoner, J.S., Xueliang, S., Yuan, W., Whitmore, T.J., 1999. Paleoclimate of Southwestern China for the past 50,000 yr inferred from lake sediment records. Quat. Res. 52, 369–380.
- Hollander, D.J., Smith, M.A., 2001. Microbially mediated carbon cycling as a control on the ¹³C of sedimentary carbon in eutrophic Lake Mendota (USA): new models for interpreting isotopic excursions in the sedimentary record. Geochem. Cosmochim. Acta 65, 4321–4337.
- Horita, J., Wesolowski, D., 1994. Liquid-vapour fractionation of oxygen and hydrogen isotopes of water from the freezing to the critical temperature. Geochim. Cosmochim. Acta 47, 3425–3437.
- Horton, T.W., Defliese, W.F., Tripati, A.K., Oze, C., 2016. Evaporation induced ¹⁸O and ¹³C enrichment in lake systems: a global perspective on hydrologic balance effects. Quat. Sci. Rev. 131, 365–379.
- Hou, J., D'Andrea, W.J., Wang, M., He, Y., Liang, J., 2017. Influence of the Indian monsoon and the subtropical jet on climate change on the Tibetan Plateau since the late Pleistocene. Quat. Sci. Rev. 163, 84–94.
- Hu, C., Henderson, G.M., Huang, J., Xie, S., Sun, Y., Johnson, K.R., 2008. Quantification of Holocene Asian monsoon rainfall from spatially separated cave records. Earth Planet. Sci. Lett. 266, 221–232.
- IAEA/WMO, 2018. Global Network of Isotopes in Precipitation. The GNIP Database. Karamperidou, C., DiNezio, P.N., Timmerman, A., Jin, F.-F., Cobb, K.M., 2015. The response of ENSO flavors to mid-Holocene climate: implications for proxy interpretation. Paleoceanography 30, 527–547.
- Kim, S.-T., O'Neil, J.R., 1997. Equilibrium and nonequilibrium oxygen isotope effects in synthetic carbonates. Geochem. Cosmochim. Acta 61, 3461–3475.
- Kottek, M., Grieser, J., Beck, C., Rudolf, B., Rubel, F., 2006. World Map of the Köppen-Geiger climate classification updated. Meteorol. Z. 15, 259–263.

- Koutavas, A., deMenocal, P.B., Olice, G.C., Lynch-Stieglitz, J., 2006. Mid-Holocene El Niño–Southern Oscillation (ENSO) attenuation revealed by individual foraminifera in eastern tropical Pacific sediments. Geology 34, 993–996.
- Kudrass, H.R., Hofmann, A., Doose, H., Emeis, K., Erlenkeuser, H., 2001. Modulation and amplification of climatic changes in the Northern Hemisphere by the Indian summer monsoon during the past 80 k.y. Geology 29, 63–66.
- Kumar, K.K., Rajagopalan, B., Hoerling, M., Bates, G., Cane, M., 2006. Unraveling the mystery of Indian monsoon failure during El Nino. Science 314, 115–119.
- Kutzbach, J., 1981. Monsoon climate of the early Holocene: climate experiment with the earth's orbital parameters for 9000 years ago. Science 214, 59–61.
- Laskar, J., Robutel, P., Joutel, F., Gastineau, M., Correia, A.C.M., Levrard, B., 2004.
 A long-term numerical solution for the insolation quantities of the Earth. Astron.
 Astrophys. 428, 261–285.
- Leng, M.J., Wagner, B., Boehm, A., Panagiotopoulos, K., Vane, C.H., Snelling, A., Haidon, C., Woodley, E., Vogel, H., Zanchetta, G., Baneschi, I., 2013. Understanding past climatic and hydrological variability in the Mediterranean from Lake Prespa sediment isotope and geochemical record over the Last Glacial cycle. Quat. Sci. Rev. 66. 123–136.
- Li, H.-C., Ku, T.-L., 1997. δ^{13} C- δ^{18} O covariance as a paleohydrological indicator for closed-basin lakes. Palaeogeogr. Palaeoclimatol. Palaeoecol. 133, 69–80.
- Liu, X., Liu, Z., Kutzbach, J., Clemens, S.C., Prell, W.L., 2006. Hemispheric insolation forcing of the Indian Ocean and Asian Monsoon: local versus Remote Impacts. J. Clim. 16, 6195–6208.
- Liu, J., Chen, J., Zhang, X., Li, Y., Rao, Z., Chen, F., 2015. Holocene East Asian summer monsoon records in northern China and their inconsistency with Chinese stalagmite δ¹⁸Orecords. Earth-Sci. Rev. 148, 194–208.
- Liu, J., Ren, H.-L., Li, W., Zuo, J., 2018. Remarkable impacts of Indian Ocean Sea surface temperature on interdecadal variability of Summer rainfall in Southwestern China. Atmosphere 9 (103).
- Löwemark, L., Chen, H.F., Yang, T.N., Kylander, M., Yu, E.F., Hsu, Y.W., Lee, T.Q., Song, S.R., Jarvis, S., 2011. Normalizing XRF-scanner data: a cautionary note on the interpretation of high-resolution records from organic-rich lakes. J. Asian Earth Sci. 40, 1250–1256.
- Lu, Z., Liu, Z., Zhu, J., Cobb, K.M., 2018. A Review of Paleo El Niño-Southern Oscillation. Atmosphere 9, 130.
- Meyers, P., 1994. Preservation of elemental and isotopic source identification of sedimentary organic matter. Chem. Geol. 114, 289–302.
- Misra, P., Tandon, S.K., Sinha, R., 2019. Holocene climate records from lake sediments in India: Assessment of coherence across climate zones. Earth Sci. Rev. 190, 370–397.
- Morrill, C., Overpeck, J.T., Cole, J.E., Liu, K.-B., Shen, C., Tang, L., 2006. Holocene variations in the Asian monsoon inferred from the geochemistry of lake sediments in Central Tibet. Quat. Res. 65, 232–243.
- Mortimer, R.J.G., Coleman, M.K., 1997. Microbial influence on the oxygen isotopic composition of diagenetic siderite. Geochem. Cosmochim. Acta 61, 1705–1711.
- Olsson, I., 1986. Radiometric methods. In: Berglund, B. (Ed.), Handbook of Holocene Palaeoecology and Palaeohydrology. John Wiley and Sons, Chichester, pp. 273–312.
- Pausata, F.S.R., Zhang, Q., Muschitiello, F., Lu, Z., Chafik, L., Niedermeyer, E.M., Stager, J.C., Cobb, K.M., Liu, Z., 2017. Greening of the Sahara suppressed ENSO activity during the mid-Holocene. Nat. Commun. 8, 1–12.
- Prasad, S., Anoop, A., Riedel, N., Sarkar, S., Menzel, P., Basavaiah, N., Krishnan, R., Fuller, D., Plessen, B., Gaye, B., Röhl, U., Wilkes, H., Sachse, D., Sawant, R., Wiesner, M.G., Stebich, M., 2014. Prolonged monsoon droughts and links to Indo-Pacific warm pool: a Holocene record from Lonar Lake, Central India. Earth Planet. Sci. Lett. 391, 171–182.
- R Core Development Team, 2008. R: A Language and Environment for Statistical Computing.
- Rao, Z., Li, Y., Zhang, J., Jia, G., Chen, F., 2016. Investigating the long-term palaeoclimatic controls on the δD and $\delta^{18}O$ of precipitation during the Holocene in the Indian and East Asian monsoonal regions. Earth Sci. Rev. 159, 292–305.
- Ratna, S.B., Cherchi, A., Osborn, T.J., Joshi, M., Uppara, U., 2021. The extreme positive Indian Ocean dipole of 2019 and associated Indian summer monsoon rainfall response. Geophys. Res. Lett. 48 e2020GL091497.
- Reimer, P.J., Austin, W.E.N., Bard, E., Bayliss, A., Blackwell, P.G., Bronk Ramsey, C., Butzin, M., Cheng, H., Edwards, R.L., Friedrich, M., Grootes, P.M., Guilderson, T.P., Hajdas, I., Heaton, T.J., Hogg, A.G., Hughen, K.A., Kromer, B., Manning, S.W., Muscheler, R., Palmer, J.G., Pearson, C., van der Plicht, J., Reimer, R.W., Richards, D.A., Scott, E.M., Southon, J.R., Turney, C.S.M., Wacker, L., Adolphi, F., Büntgen, U., Capano, M., Fahrni, S.M., Fogtmann-Schulz, A., Friedrich, R., Köhler, P., Kudsk, S., Miyake, F., Olsen, J., Reinig, F., Sakamoto, M., Sookdeo, A., Talamo, S., 2020. The INTCAL20 Northern Hemisphere radiocarbon age calibration curve (0–55 cal kBP). Radiocarbon 1–33.
- Rozanski, K., Araguás-Araguás, L., Gonfiantini, R., 1993. Isotopic patterns in modern global precipitation. In: Swart, P.K., Lohmann, K.C., Mckenzie, J., Savin, S. (Eds.), Climate Change in Continental Isotopic Records. American Geophysical Union, Washington, D.C.
- Sharmila, S., Joseph, S., Sahai, A.K., Abhilash, S., Chattopadhyay, R., 2015. Future projection of Indian summer monsoon variability under climate change scenario: an assessment from CMIP5 climate models. Glob. Planet. Chang. 124, 62–78.
- Shen, J., Jones, R.T., Yang, X., Dearing, J.A., Wang, S., 2006. The Holocene vegetation history of Lake Erhai, Yunnan province southwestern China: the role of climate and human forcings. The Holocene 16, 265–276.
- Song, X.-Y., Yao, Y.-F., Wortley, A.H., Paudayal, K.N., Yang, S.-H., Li, C.-S., Blackmore, S., 2012. Holocene vegetation and climate history at Haligu on the Jade Dragon Snow Mountain, Yunnan, SW China. Clim. Chang. 113, 841–866.
- Steinman, B., Rosenmeier, M.F., Abbott, M.B., Bain, D.J., 2010. The isotopic and hydrologic response of small, closed basin lakes to climate forcing from predictive

- models: application to paleoclimate studies in the upper Columbia River basin. Limnol. Oceanogr. 55, 2231-2245.
- van Dijk, J., Fernandez, A., Muller, I.A., Lever, M., Bernasconi, S.M., 2019. Oxygen isotope fractionation in the siderite-water system between 8.5 and 62 °C. Geochim. Cosmochim. Acta 220, 535–551.
- Vuille, M., Werner, M., Bradley, R.S., Keimig, F., 2005. Stable isotopes in precipitation in the Asian monsoon region. J. Geophys. Res. 110.
- Wang, E., Burchfiel, B.C., Royden, L.H., Liangzhong, C., Jishen, C., Wenxin, L., Zhiliang, C., 1998. Late Cenozoic Xianshuihe-Xiaojiang, Red River, and Dali Fault Systems of Southwestern Sichuan and Central Yunnan. Special Paper of the Geological Society of America, China, p. 327.
- Wang, Y., Cheng, H., Edwards, R.L., He, Y., Kong, X., An, Z., Wu, J., Kelly, M.J., Dykoski, C.A., Li, X., 2005. The Holocene Asian monsoon: links to solar changes and North Atlantic climate. Science 308, 854–857.
- Wang, Y., Cheng, H., Edwards, R.L., Kong, X., Shao, X., Chen, S., Wu, J., Jiang, X., Wang, X., An, Z., 2008. Millennial- and orbital-scale changes in the East Asian monsoon over the past 224,000 years. Nature 451, 1090–1093.
- Wang, Y., Bekeschus, B., Handorf, D., Liu, X., Dallmeyer, A., Herzschuh, U., 2017. Coherent tropical-subtropical Holocene see-saw moisture patterns in the Eastern Hemisphere monsoon systems. Quat. Sci. Rev. 169, 231–242.
- Wang, J.K., Johnson, K.R., Borsato, A., Amaya, D.J., Griffiths, M.L., Henderson, G.M., Frisia, S., Mason, A., 2019. Hydroclimatic variability in Southeast Asia over the past two millennia. Earth Planet. Sci. Lett. 525.
- Whitmore, T.J., Brenner, M., Jiang, Z., Curtis, J.H., Moore, A.M., Engstrom, D.R., Yu, W., 1997. Water quality and sediment geochemistry in lakes of Yunnan Province, southern China. Environ. Geol. 32, 45–55.
- Wittkop, C., Teranes, J., Lubenow, B., Dean, W.E., 2014. Carbon- and oxygen-stable isotopic signatures of methanogenesis, temperature, and water column stratification in Holocene siderite varves. Chem. Geol. 389, 153–166.
- Wright, H., Mann, D., Glaser, P., 1984. Piston corers for peat and lake sediments. Ecology
- Wu, D., Zhou, A., Liu, J., Chen, X., Wei, H., Sun, H., Yu, J., Bloemendal, J., Chen, F., 2014. Changing intensity of human activity over the last 2,000 years recorded by the magnetic characteristics of sediments from Xingyun Lake, Yunnan, China. J. Paleolimnol. 53, 47–60.
- Wu, D., Chen, X., Lv, F., Brenner, M., Curtis, J., Zhou, A., Chen, J., Abbott, M., Yu, J., Chen, F., 2018. Decoupled early Holocene summer temperature and monsoon precipitation in Southwest China. Quat. Sci. Rev. 193, 54–67.

- Xiao, X., Haberle, S.G., Yang, X., Shen, J., Han, Y., Wang, S., 2014. New evidence on deglacial climatic variability from an alpine lacustrine record in northwestern Yunnan Province, southwestern China. Palaeogeogr. Palaeoclimatol. Palaeoecol. 406, 9–21
- Xiao, X., Shen, J.I., Haberle, S.G., Han, Y., Xue, B., Zhang, E., Wang, S., Tong, G., 2015.
 Vegetation, fire, and climate history during the last 18500 cal BP in south-western Yunnan Province, China. J. Quat. Sci. 30, 859–869.
- Xiao, X., Haberle, S.G., Li, Y., Liu, E., Shen, J., Zhang, E., Yin, J., Wang, S., 2017. Evidence of Holocene climatic change and human impact in northwestern Yunnan Province: high-resolution pollen and charcoal records from Chenghai Lake, southwestern China. The Holocene 28, 127–139.
- Xiao, X., Yao, A., Hillman, A., Shen, J., Haberle, S.G., 2020. Vegetation, climate and human impact since 20 ka in Central Yunnan Province based on high-resolution pollen and charcoal records from Dianchi, southwestern China. Quat. Sci. Rev. 236.
- Xu, H., Zhou, X., Lan, J., Liu, B., Sheng, E., Yu, K., Cheng, P., Wu, F., Hong, B., Yeager, K. M., Xu, S., 2017. Late Holocene Indian Summer Monsoon variations recorded at Lake Erhai, Southwestern China. Quat. Res. 83, 307–314.
- Yan, D., Wunnemann, B., Jiang, Z., 2020. Hydrological variations of a lake-catchment and human interaction during the last 6 ka in Yunnan, China. J. Hydrol. 587, 124932.
- Yang, Y., Zhang, H., Chang, F., Meng, H., Pan, A., Zheng, Z., Xiang, R., 2016. Vegetation and climate history inferred from a Qinghai Crater Lake pollen record from Tengchong, southwestern China. Palaeogeogr. Palaeoclimatol. Palaeoecol. 461, 1–11
- Yang, X., Yang, H., Wang, B., Huang, L.-J., Shen, C.-C., Edwards, R.L., Cheng, H., 2019. Early-Holocene monsoon instability and climatic optimum recorded by Chinese stalagmites. The Holocene 29, 1059–1067.
- Yuan, Y., Yang, S., 2012. Impacts of different types of El Niño on the East Asian climate: focus on ENSO cycles. J. Clim. 25, 7702–7722.
- Yuan, Z., Wu, D., Niu, L., Ma, X., Li, Y., Hillman, A.L., Abbott, M.B., Zhou, A., 2021. Contrasting ecosystem responses to climatic events and human activity revealed by a sedimentary record from Lake Yilong, southwestern China. Sci. Total Environ. 783, 146922.
- Zhang, C.L., Horita, J., Cole, D.R., Zhou, J., Lovley, D.R., Phelps, T.J., 2001. Temperature-dependent oxygen and carbon isotope fractionations of biogenic siderite. Geochem. Cosmochim. Acta 65, 2257–2271.
- Zhao, C., Cheng, J., Wang, J., Yan, H., Leng, C., Zhang, C., Feng, Z., Liu, W., Yang, X., Shen, J., 2021. Paleoclimate significance of reconstructed rainfall isotope changes in Asian Monsoon Region. Geophys. Res. Lett. 48 e2021GL092460.